FORECASTING MESOSCALE CONVECTIVE COMPLEX MOVEMENT IN CENTRAL SOUTH AMERICA

Marc R. Gasbarro

551st Electronic Systems Wing
Electronic Systems Center
Hanscom AFB, Massachusetts

Ronald P. Lowther

Air and Space Science Directorate
Air Force Weather Agency
Offutt AFB, Nebraska

Stephen F. Corfidi

NOAA/National Weather Service
Storm Prediction Center
Norman, Oklahoma

Abstract

A method for operationally predicting the movement of the centroid, or coldest cloud tops, of mesoscale convective complexes (MCCs) in Central South America (CSA) is presented (Gasbarro 2003). The procedure of predicting the movement of an MCC centroid, which primarily relates to the area of heaviest precipitation within the MCC, is modified from the work of Corfidi et al. (1996). This process is based on the concept that the motion of quasi-stationary or backward-propagating convective systems can be found as the sum of the advective component, defined by the mean motion of the cells comprising the system, and the propagation component, defined by the rate and location of new cell formation relative to existing cells. These concepts and the forecast procedure are examined using 22 mesoscale convective systems (MCSs), 20 of which were classified as MCCs.*

It is found that the advective component of MCS motion is well correlated to the mean flow in the cloud layer. Similarly, the propagation component is shown to be directly proportional, but opposite in sign, and well correlated to the direction of the low-level jet. Correlation coefficients between forecast and observed values for the speed and direction of the MCSs and MCCs for CSA are 0.72 and 0.81, respectively. This compares well to correlation coefficients of 0.80 and 0.78 for the MCC or MCS speeds and directions, respectively, of the CFM96 method for North American MCC and MCS movement. Mean absolute errors of the centroid speed and direction are 2.1 m s^{-1} and 16.4° respectively. These errors, comparing well to the CFM96 method, are sufficiently small so that the forecast path of the centroid would be well within the heavy rain swath of a typical MCC.

1. Introduction

Mesoscale convective complexes (MCCs) are responsible for producing severe weather and flooding rains in Central South America (CSA). This region includes Paraguay, Uruguay, Northern Argentina, and Southeastern Brazil (Velasco and Fritsch 1987). They are responsible for producing damaging winds, hail, injuries, and occasionally even deaths. Furthermore, MCCs significantly change and/or influence upper-atmospheric wind fields, presenting problems with aviation safety and efficiency problems with flight scheduling (CFM96). In addition, the sparse data network of South America (SA) further adds to the difficulty of accurately forecasting MCC movement due to the lack of synoptic observations.

There are many similarities between North America (NA) and SA MCCs (Velasco and Fritsch 1987). As in NA, SA MCCs are nocturnal storms that owe their existence partly due to a moist, poleward advecting low-level jet (LLJ) that is comparable in strength to the United States (US) LLJ. The steep Andes mountain chain helps to initiate convection and channel the South American low-level jet (SALLJ) (Saulo et al. 2000) poleward. This process is similar to the process associated with the North American LLJ in the lee of the Rocky Mountains. Like NA MCCs, those in SA form mainly during the warm season [November through April in the southern hemisphere (SH)]. SA MCCs generally exhibit a similar dynamic structure to NA MCCs. MCCs in both hemispheres usually require the presence of a quasi-stationary

*Cordifi et al. (1996) will be referred to as "CFM96" for the remainder of this paper.

boundary associated with moderately intense, transient upper-level shortwaves. The shortwaves promote storm development by destabilizing the atmosphere and enhancing upper-level divergence. MCCs require minimal upper-level shear; therefore, very strong shortwaves are not conducive to MCC growth. Surface temperatures on both continents are similar around the location of MCC genesis. Finally, the favored region of MCC genesis in both NA and SA shifts westward throughout the warm season months as the respective North or South Atlantic subtropical highs build westward (Velasco and Fritsch 1987).

SA MCCs also exhibit various differences from their NA counterparts (Velasco and Fritsch 1987). One major difference is size. SA MCCs are, on average, 60% larger than NA MCCs. Velasco and Fritsch (1987) found that the average size of the -32°C cloud shield in SA MCCs is around 400,000 km², compared to only 300,000 km² for NA. SA MCC lifespan averages 11.5 hours vs. 9 to 9.5 hours in NA (Maddox et al. 1986; Velasco and Fritsch 1987). SA MCCs form more equatorward and with less latitudinal variability than NA MCCs. NA MCCs generally form from 30° to 50° N, while MCCs in SA typically are generated only between 25° and 35° S. Unlike in NA, SA MCCs are present into late austral summer and early autumn (Velasco and Fritsch 1987). Surface dewpoints in which MCCs spawn are 3-5°C higher in SA than in NA (Davison 1999; Velasco and Fritsch 1987). Also, the tropopause in SA MCCs averages about 100 mb vs. 150 to 200 mb in NA (Velasco and Fritsch 1987). A higher tropopause along with higher surface dewpoints implies greater thermodynamic instability associated with MCCs in SA. The moisture source region for SA MCCs also aids in fueling very unstable conditions. In NA, the moisture source for the LLJ is the Gulf of Mexico; however, rather than a body of water, the SALLJ feeds off the Amazon Basin, a very warm, shallow, land moisture source. Finally, the SALLJ owes its existence mainly due to a tight pressure gradient between a thermal low, the North Argentine Depression, and the South Atlantic High (Saulo et al. 2000). This differs from NA where the US LLJ principally forms from boundary layer frictional differences and a nocturnal inversion (Bonner 1968). Consequently, the SALLJ lasts longer in the day and occurs more frequently than in NA (Velasco and Fritsch 1987).

Various synoptic features in SA working in cohesion generate conditions necessary for MCC formation. Climatologically, the North Argentine Depression and the South Atlantic High are present through the austral warm season (Fig. 1) (Lenters and Cook 1999). When one or both of the two pressure features intensify, the pressure gradient between the two systems tightens, which increases the intensity of the SALLJ and the low-level and moisture flux convergence (Saulo et al. 2000). Quasi-stationary boundaries such as slow moving fronts, squall lines, and the South Atlantic Convergence Zone (SACZ) (Fig. 1) greatly enhance low-level convergence (Lenters and Cook 1999). These ingredients, combined with tremendous

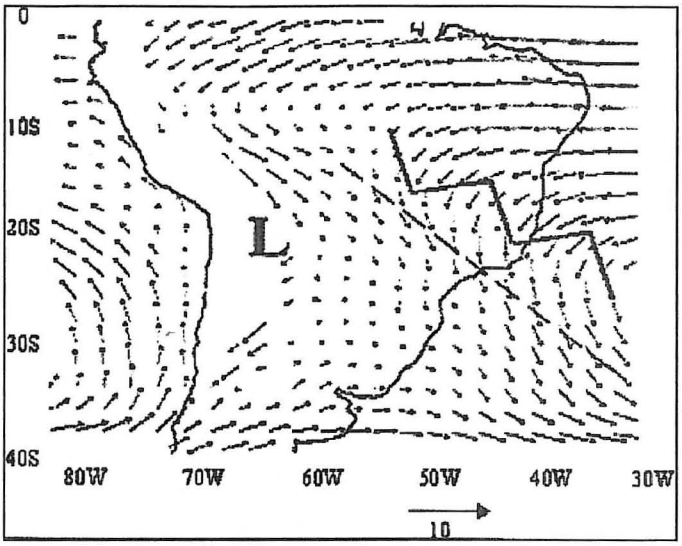

Fig. 1. Mean positions of the North Argentine Depression, South Atlantic Convergence Zone (dashed line), South Atlantic ridge (zigzag line), and 850 mb fectors (m s^{-1}) during December to February (modified from Lenters and Cook 1999).

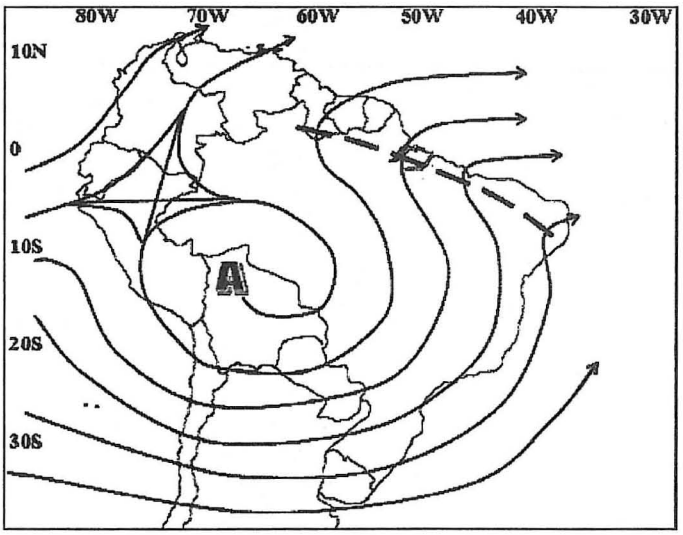

Fig. 2. Mean 200 mb position of the Bolivian High for January (modified from Davison 1999).

outflow in the upper levels (Fig. 2), create conditions for MCC development and intensification. In addition, increases in the strength of the Bolivian High, an upper-level high climatologically centered over Bolivia, relate to a stronger STJ (Fig. 2). A stronger jet crossing the Andes leads to increased shortwave perturbations, which ultimately helps initiate MCSs and MCCs (Davison 1999).

CFM96 proposed a method to determine movement of MCCs in NA using the principle that movement of MCCs is affected by both cloud layer advection and propagation components. CFM96 hypothesized that the advective component of MCC movement is proportional to the mean cloud layer flow. They also hypothesized that the propagation component is equal and opposite of the LLJ. After successfully verifying that both components do significantly influence MCC

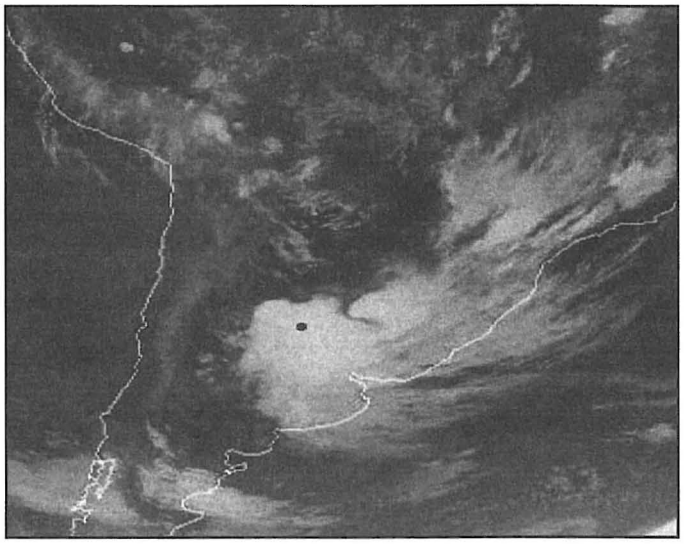

Fig. 3. MCC over South America at 0245 UTC 25 Nov 2002. Black dot represents the centroid of the system (coldest cloud tops) (modified from CIRA 2002).

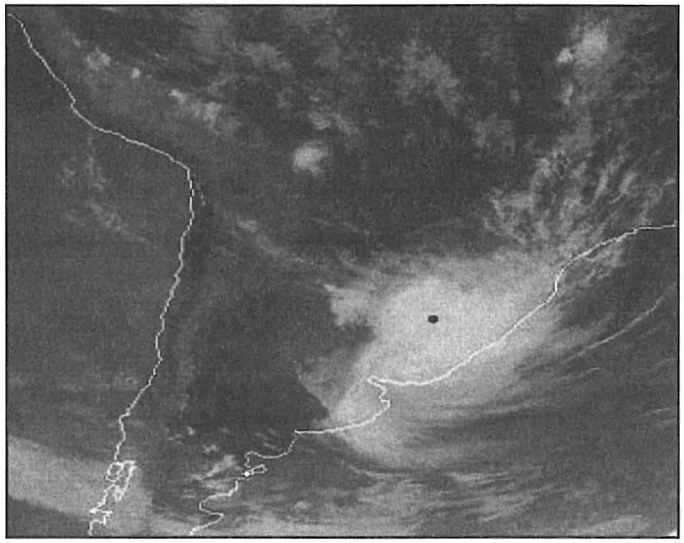

Fig. 4. As in Fig. 3, except for 1145 UTC 25 Nov 2002.

movement, CFM96 verified this empirical technique by correlating the forecasted MCC vector, a summation of both the advective and propagation vectors, to the actual MCC vector.

A method similar to CFM96 can be applied to South American MCCs by utilizing the same principle described above. The verification of this research's results, however, differs from the CFM96 verification. CFM96 verified their results by tracking the meso-beta scale convective elements responsible for the heaviest rainfall. Due to a lack of available radar imagery from SA, this study will not track MCCs based on radar-observed movements. Instead, this research verifies MCC movement by measuring the movement of the MCC cold cloud shield centroid from Geostationary Operational Environmental Satellite (GOES) infrared (IR) satellite imagery. Maddox (1980) states that the coldest cloud tops relate to the areas of most intense precipitation. Since intense precipitation relates to increased radar echo returns, this research produces results comparable to those of CFM96.

Sections 2 and 3 describe the methodology and results for validating the advective and propagation components, and then verify the forecasted MCC movement against the actual MCC movement. A brief summary along with concluding remarks are given in Section 4.

2. Data and Methodology

Twenty-two MCC and MCS cases were analyzed to verify the CFM96 method of MCC movement for SA. Two of the cases are in January 2001 with the remainder from September to December 2002. Twenty of the 22 cases are MCCs. The International Desks section of the Hydrometeorological Prediction Center (HPC) at the NOAA/National Center for Environmental Prediction (NCEP) provided GOES-8 satellite imagery for the 2001 case studies (Davison 2002), while the Cooperative Institute for Research in the Atmosphere (CIRA) provided GOES-8 satellite imagery for the 2002 cases (CIRA 2002). This study only utilized three-hourly, channel four IR imagery for the detection of cold cloud tops.

Due to very sporadic and inconsistent upper air sounding data in the region of study, this research utilized upper air reanalysis data from the Fleet Numerical Meteorological and Oceanography Detachment (FNMOD), Asheville, NC, for verification of the CFM96 method. The U.S. Navy runs the Navy Operational Global Atmospheric Prediction System (NOGAPS) model to produce reanalysis data twice per day at 0000 and 1200 UTC. The FNMOD in Asheville, NC, stores the archived NOGAPS reanalysis data for future use.

Satellite imagery was used to track 20 MCCs and 2 MCSs by tracking the centroid of the system. Only satellite images meeting MCC criteria and very large MCSs were used in this study. The black dots in Figs. 3 and 4 show the position of the centroid over nine hours. The dots represent the center of the coldest cloud tops.

The actual distance, direction, and speed of the MCC was determined by first interpolating the latitude and longitude of the black dots from satellite imagery. The starting and ending latitude and longitude were then converted to distance and azimuthal angle following the method described by Snyder (1987).

Individual cells that would eventually intensify into MCCs or large MCSs were also tracked using the same method. However, having only one satellite image for every 3 hours time, it was very difficult to discern between individual cells and a coalesced cluster of cells. Only 12 of the 22 cases produced cells distinctly visible for two consecutive three-hourly images. The speeds and directions of the 12 cases were then compared to the 850-300 mb mean flow to verify that cells move downwind with respect to the velocity of the mean flow. If it is true, this suggests that mean cloud layer velocity would not only affect the movement of

the individual cells, but of the MCCs and MCSs as well (CFM96).

Winds associated with the MCC or MCS are necessary for implementation of the CFM96 method. Upper level wind speed and direction at the location of MCC or MCS genesis were interpolated from 850, 700, 500, and 300 mb NOGAPS wind vector reanalysis charts. This technique differs from the CFM96 method of utilizing the nearest rawinsonde station. As in the CFM96 method, this study utilized the 0000 UTC wind data since 0000 UTC usually occurred within six hours of MCC or MCS genesis. Per CFM96, the wind speeds and directions of each level were then inserted into Eqs. 1 and 2, respectively, to produce the mean advective cloud layer flow component of MCC or MCS motion. This component (S_{CL} for speed and DIR_{CL} for direction), called the advective component, is the mean 850-300 mb wind velocity that advects the system downwind (Fig. 5). To arrive at a representable mean direction, 360° was added to any 850 and 700 mb wind direction between 001° and 180°. This was done because it is not uncommon for low-level winds to occur from the north to northeast. For example, averaging a very low direction number (i.e. 020°) with a high direction number (i.e. 330°) incorrectly skewed the average directional component. The following equations are used to produce the mean advective cloud layer component of the MCC or MCS:

$$S_{CL} = \frac{(S_{850} + S_{700} + S_{500} + S_{300})}{4} \quad (1)$$

$$DIR_{CL} = \frac{(DIR_{850} + DIR_{700} + DIR_{500} + DIR_{300})}{4} \quad (2)$$

CFM96 hypothesized that storms propagate further with stronger LLJs. Although factors such as orographic influences, thermodynamic instability, and outflow boundaries influence propagation, storms mainly form and regenerate in the exit region of the LLJ due to low-level mass and moisture flux convergence. CFM96 found the propagation component equal in magnitude, but opposite in direction to the low-level inflow or LLJ (Fig. 5). In this research, the maximum wind speed and direction near the location of MCC or MCS genesis were interpolated from 850 mb NOGAPS vector reanalysis charts. Since MCCs typically propagate toward the level of inflow or into the LLJ, this study used the maximum wind speed at 850 mb within 100 nm upwind of the MCC or MCS genesis region.

While CFM96 strictly followed Bonner's (1968) criteria for the LLJ, this study assumed a LLJ level of 850 mb for all events. This was a valid assumption since Saulo et al. (2000) found the average maximum wind speed associated with the SALLJ to occur approximately at 850 mb. Among LLJ occurrences, Saulo et al. (2000) found an average of 20 m s^{-1} at 850 mb compared against an average of 8 m s^{-1} at 700 mb.

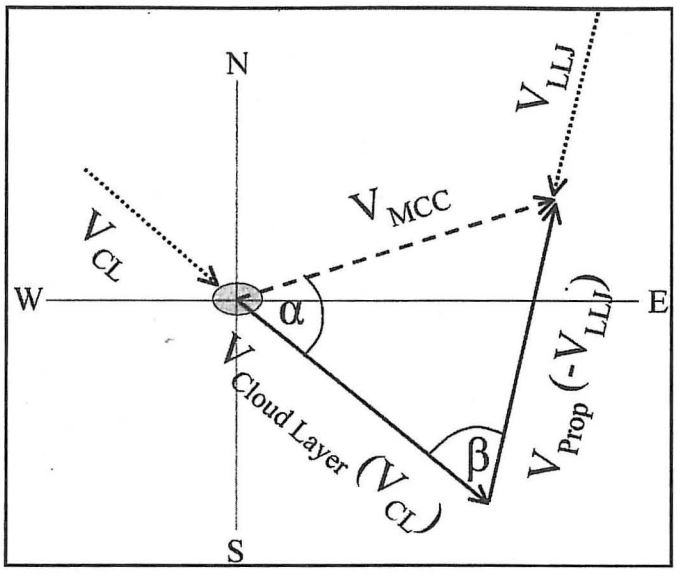

Fig. 5. Conceptual model of the vector components and angles used to predict MCC or MCS velocity, V_{MCC}. The magnitude and direction of the propagation component, V_{PROP} are equal and opposite to the low-level jet, V_{LLJ}. Angles α and β are related to the forecasted MCC or MCS direction and are calculated in Eqs. 7 and 5, respectively. The V_{MCC} vector is the forecasted MCC or MCS motion. V_{MCC}, calculated in Eq. 6, is the vector sum of the V_{CL} and V_{PROP} components. The circle at the intersection of the E-W and N-S axes denotes the starting MCC or MCS location.

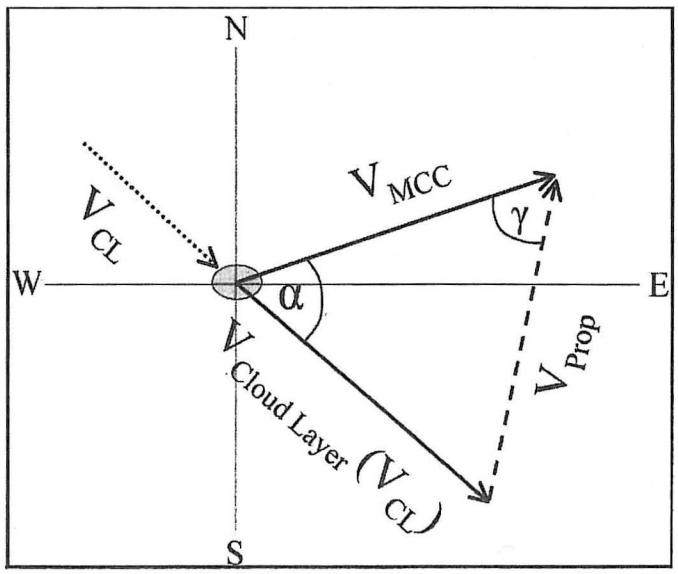

Fig. 6. Conceptual model of the vector components and angles used to predict propagation velocity, V_{PROP}. The V_{MCC} vector is the observed MCC or MCS motion. V_{PROP}, computed in Eq. 3, is the vector sum of the V_{CL} and V_{MCC} components. Angle α represents the difference in direction between V_{CL} and V_{MCC}. Angle γ, calculated in Eq. 4, is related to the propagation direction. The circle at the intersection of the E-W and N-W axes denotes the starting MCC or MCS location.

Since Saulo et al. based their findings by meticulously following Bonner's criteria, this research used 850 mb as a representable level of maximum inflow.

This research followed the CFM96 procedure in verifying the relationship between the direction of the

LLJ and the direction of propagation. To verify that the LLJ and propagation components are 180° different in direction with each other, the propagation component, V_{PROP}, must be calculated by inserting the observed mean advective component speed, S_{CL}, observed MCC or MCS speed, S_{MCC}, and angle, α, into Eq. 3. Figure 6 illustrates how angle, α, between the observed mean cloud layer wind and observed MCC motion vectors influences the magnitude of the propagation component. Equation 4 then uses the calculated propagation component, V_{PROP}, to determine the angle between the actual MCC motion and the propagation component. Figure 6 depicts how this angle, γ, relates to the actual direction of propagation. If a strong correlation between the actual propagation and LLJ vectors exists, then this suggests that the LLJ is a very good indicator of the direction of propagation of MCC and MCS movement.

$$V_{PROP} = \sqrt{(S_{CL})^2 + (S_{MCC})^2 - 2(S_{CL})(S_{MCC})\cos(\alpha)} \quad (3)$$

$$\gamma = \arccos\left[\frac{(S_{CL})^2 - (S_{MCC})^2 - (V_{PROP})^2}{-2(S_{MCC})(V_{PROP})}\right] \quad (4)$$

After showing that both advective and propagation components relate to the mean flow and LLJ respectively, a relationship between forecasted and observed MCC or MCS speed and direction is formulated. This relationship serves to demonstrate that forecasted MCC and MCS motion verify against the actual movement of MCCs and MCSs.

Solving Eqs. 5 through 7 creates a forecast of MCC or MCS movement. To compute the magnitude of the system speed, the β angle must first be computed. The β angle, illustrated in Fig. 5 and computed in Eq. 5, is simply the angle between the mean advective and propagation components. For proper representation, the LLJ, DIR_{LLJ}, and mean cloud layer flow (DIR_{CL}) were subtracted from 360°. For Eq. 5 to work, 360° is added to either variable if the direction is between 001° and 180°. Next, the angle along with the LLJ and mean cloud layer wind speeds, S_{LLJ} and S_{CL}, respectively, are inserted into Eq. 6 to arrive at the predicted velocity of the MCC or MCS, V_{MCC}. Finally, the LLJ speed, mean cloud layer wind speed, and predicted MCC or MCS velocities, S_{LLJ}, S_{CL}, and V_{MCC} respectively, are inserted into Eq. 7 to determine the angle, α, between the cloud layer flow and predicted MCC movement. This angle directly relates to the actual direction in which the convective system is heading (Fig. 5).

$$\beta = (360 - DIR_{CL}) - (360 - DIR_{LLJ}) \quad (5)$$

$$V_{MCC} = \sqrt{(S_{CL})^2 + (S_{LLJ})^2 - 2(S_{CL})(S_{LLJ})\cos(\beta)} \quad (6)$$

$$\alpha = \arccos\left[\frac{(S_{LLJ})^2 - (V_{MCC})^2 - (S_{CL})^2}{-2(V_{MCC})(S_{CL})}\right] \quad (7)$$

The process for determining predicted MCC or MCS motion differs slightly from the CFM96 method. As illustrated in Figs. 5 and 6, simple right-angle trigonometry does not apply in determining magnitudes and directions. CFM96 calculated all angles and magnitudes using the law of sines and cosines; however, the CFM96 method can lead to ambiguity. Because sine is positive in both the first and second quadrant, any angle over 90° produces erroneous answers. CFM96 calculated the α angle using the law of sines. This is possible provided the angle between the advective and propagation components is not obtuse. Although obtuse angles are infrequent, they did occur in one case during this research. To eliminate confusion, this research utilized the law of cosines in Eq. 7 since cosine exhibits opposite signs within the first two Cartesian quadrants. To ensure uniformity and unambiguity, the law of cosines is also utilized in Eqs. 3, 4, and 6.

Once predicted MCC and MCS magnitudes and directions are calculated, correlations between actual and predicted values are found and compared to the CFM96 research. In addition, mean speeds, directions, and absolute errors of both observed and forecasted values are computed to compare against the CFM96 results. Standard deviations of the speeds, directions, and average absolute errors are also calculated and compared. Finally, the average absolute directional error between the observed and predicted MCC or MCS directions is translated into distances by multiplying the average absolute directional error by the average observed MCC or MCS speed and average length of time of MCC occurrence (11.5 hours in SA) (Velasco and Fritsch 1987). This result, yielding an absolute horizontal distance error, provides an estimate of the margin of error this process could exhibit.

3. Results

The CFM96 method was applied to SA and verified. The first step in verifying the CFM96 method for SA was to separately describe the results for the two components that comprise MCC and MCS movement, the advective and propagation components. After component verification, observed MCC and MCS velocities are compared against forecasted velocities. Finally, results of all findings are compared to the CFM96 method.

The actual MCC advective component (or cell speed and direction) verified very well against the mean cloud layer (850-300 mb) speed and direction. Figures 7 and 8 illustrate the correlations and scatter plots for the 12 cases for which individual cells could be tracked. Both scatter plots represent a near linear relationship between the observed cell movement and 850-300 mb mean velocity. These strong correlations mean that the advective component plays a major role in determining MCC and MCS movement.

The correlations for the advective component were comparable to those presented in the CFM96 research. This research found correlation coefficients of 0.90 and 0.87 for the speeds and directions, respectively, versus 0.71 and 0.76 for the CFM96 NA method (Table 1). A couple of hypotheses could explain the slightly stronger correlations for SA. Stronger westerlies in NA could account for larger variations in the mean flow, therefore, leading to more error in predicting cell movement. However, the more likely hypothesis concerns the difference in system height. In computing mean layer velocity, CFM96 equally weighted all four levels presented in Eqs. 1 and 2, as was done in the present study. Although mid-levels of the troposphere drive storm movement, CFM96 placed equal weight on the lowest levels, 850 and 700 mb, because most air entraining into thunderstorms enters at the lowest levels. Equal weight is also placed on the highest level, 300 mb. Use of the 300 mb level could be causing the differences in correlation coefficients between the CFM96 method and the SA method. Velasco and Fritsch (1987) found warm season tropopauses average around 100 mb in SA, 50-100 mb higher than NA tropopauses. Higher tropopauses likely contribute to the larger MCC sizes in SA (Velasco and Fritsch 1987). The higher, larger convective storms in SA would place the 300 mb level nearly in the middle of the storm's vertical extent; therefore, making 300 mb a significant steering level. On the other hand, 300 mb may not play as large of a part in steering convective cells in NA since it would lay in the top quarter to third of the storm. To summarize, the equal weight of 300mb in equations 1 and 2 may be more accurate for SA than NA. Figure 7 shows all values either near or below the line of a perfect one-to-one relationship. The plots below the line represent mean layer speeds stronger than the speeds of the cells. Some of the cells could be left-moving supercells which, analogous to right-moving supercells in the northern hemisphere, move more slowly than the mean flow when the winds back with height (veer in the northern hemisphere).

The propagation component also verified better than the CFM96 results. The scatter plot for observed propagation direction versus LLJ direction for SA is illustrated in Fig. 9 for 21 cases. One of the 22 cases was not used due to an abnormally weak LLJ speed. This figure demonstrates that the LLJ direction is a clear indication of the propagation component. In addition to better correlation coefficients [0.75 for SA vs. 0.65 for NA (Table 1)], there is much less variance in the entire population of LLJ directions. The absolute variation, maximum value minus minimum value, is only 80° for SA cases, but almost 180° for NA cases (CFM96). Less variation in the ocean-dominated SH westerlies, steeper terrain in SA, and smaller SA continent width likely caused the smaller variance among SALLJ directions.

The forecasted MCC and MCS speeds and directions compared well to the observed speeds and directions. Figures 10 and 11 depict the scatter plots for the speeds and directions respectively for all 22 cases. Both graphs exhibit a semi-linear fit of observed ver-

Table 1. Comparison of correlation coefficients between the Corfidi et al. (1996) method for North America (NA) and the author's method developed for South America (SA).

	Method for NA (Cordifi et al. method)	Method for SA (author's method)
Cell speed vs. 850-300 mb mean wind speed	0.71	0.90
Cell direction vs. 859-300 mb mean wind direction	0.76	0.87
Propagation direction vs. LLJ direction	0.65	0.75
Observed vs. forecasted MCC or MCS speed	0.80	0.72
Observed vs. forecased MCC or MCS direction	0.78	0.81

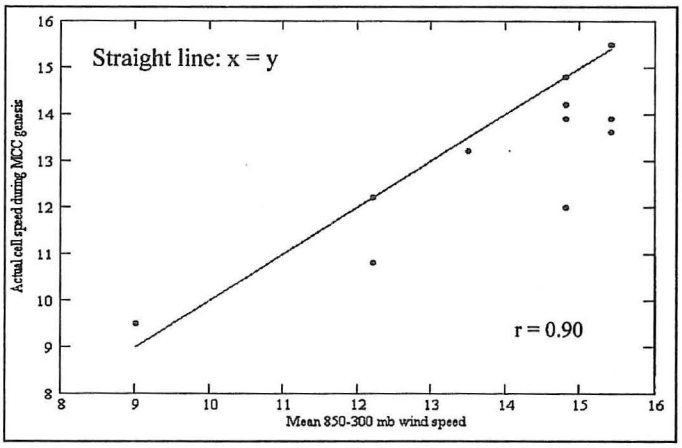

Fig. 7. Scatter plot of observed cell speed versus mean 850-300 mb wind speed for 12 cases during the MCC or MCS genesis stage. Straight line indicates a perfect (one-to-one) relationship versus measure of correlation.

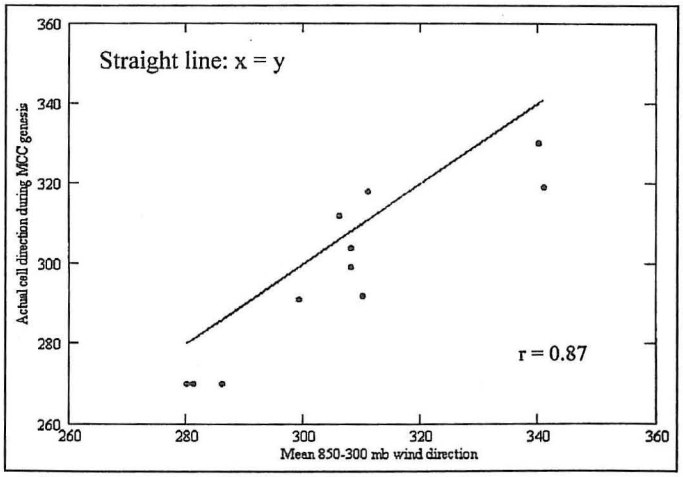

Fig. 8. As in Fig. 7, except for observed cell direction versus mean 850-300 mb wind direction for 12 cases during the MCC or MCS genesis stage.

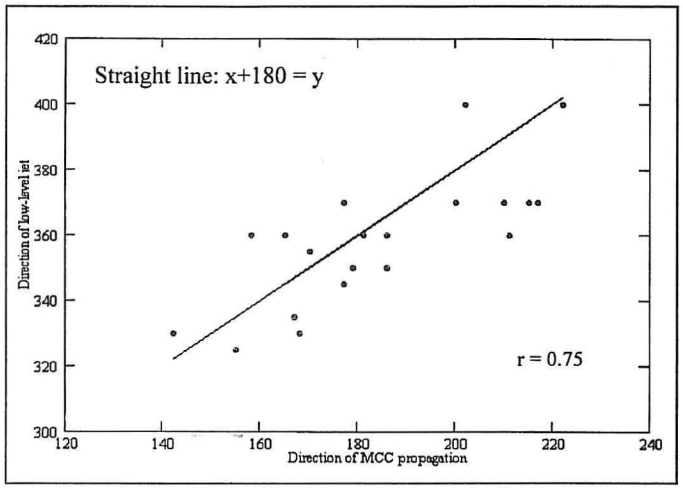

Fig. 9. Scatter plot of actual MCC and MCS propagation direction versus mean LLJ direction for 21 cases. Straight line indicates a perfect 180° relationship between the LLJ and propagation directions versus measure of correlation. LLJ directions between 000° and 040° are plotted between 360° and 400°.

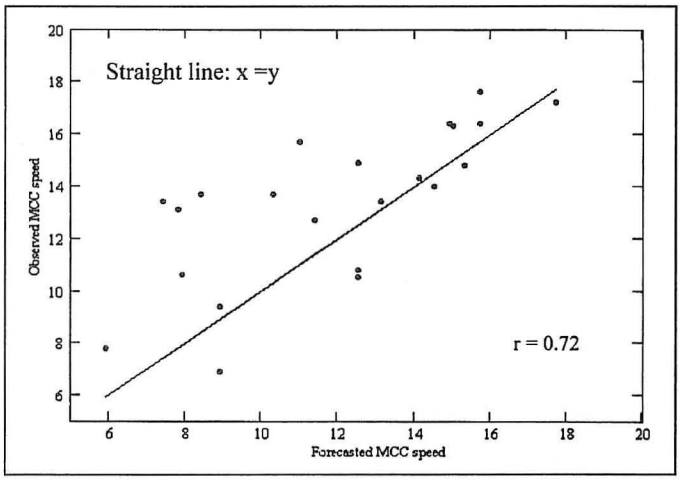

Fig. 10. Scatter plot of observed versus forecasted MCC and MCS speeds for 22 cases. Straight line indicates a perfect (one-to-one) relationship versus measure of correlation.

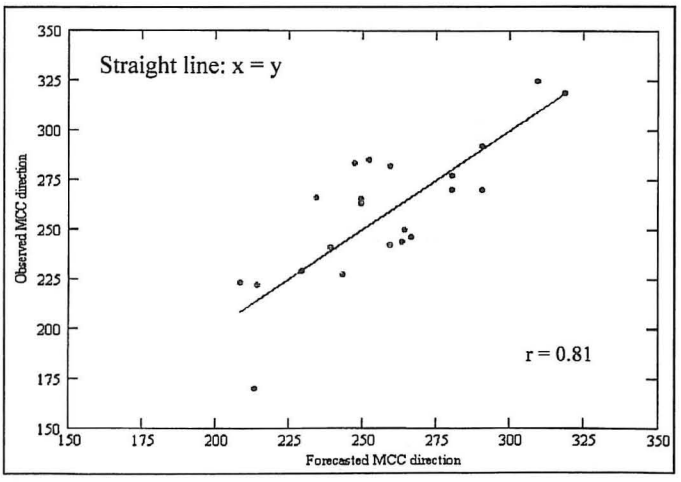

Fig. 11. As in Fig. 10, except for observed versus forecasted MCC and MCS directions for 22 cases.

sus forecasted magnitudes and directions. Correlation coefficients of 0.72 and 0.81 for the speeds and directions, respectively, for the SA method results are comparable to the CFM96 correlation coefficients of 0.80 and 0.78 for speeds and directions (Table 1).

An interesting observation in Fig. 10 is that observed speeds are mostly higher than the forecasted speeds. Values above the line in Fig. 10 represent an underforecast of the MCC or MCS speed. Synoptic scale features could account for the disparity. Several MCCs and MCSs in this study were associated with transient squall lines or fronts. Others associated themselves with moderate to strong shortwaves. Although this study does not disclose the synoptic details of each case, it is hypothesized that synoptic factors not accounted for in both the CFM96 NA method and the SA method cause faster observed motion of MCCs and MCSs. In addition, some degree of forward propagation may also have been present. This would tend to result in faster system motion (Corfidi 1998).

Observed means, standard deviations, and average absolute errors for MCC and MCS speeds of both the CFM96 NA method and the SA method are presented in Table 2. Results compare well between both methods with a couple of exceptions. Both observed and forecasted mean MCC and MCS speeds were less in SA, likely from the weaker SH westerlies inhibition of the advective component of motion. Also, the standard deviation of observed MCC and MCS speeds is less in SA than NA. The smaller variance in SH westerlies probably accounts for the smaller standard deviation for observed SA MCC and MCS speeds. In addition, MCCs and MCSs generally form from 25° to 35° S compared to NA MCCs forming between 30° and 50° N (Velasco and Fritsch 1987). The greater latitude variation in NA could also cause greater speed variances between NA MCC and MCS since mid-latitudes experience stronger effects from the polar jet than subtropical latitudes. Furthermore, SA MCCs and MCSs occur more frequently in lower latitudes where westerlies are typically weaker. To summarize, less variation in latitude and upper-level westerly speed among SA MCC and MCS cases could attribute to the lower speed standard deviation.

Comparisons between MCC and MCS directions computed from both methods also show some interesting results (Table 2). The observed and forecasted directions infer that the MCCs and MCSs move equatorward towards the moisture inflow for both hemispheres. Furthermore, the Coriolis parameter contributes to equatorward motion of the MCCs or MCSs (Bonner 1968).

The average absolute error for directions (Table 2) differs between continents. A smaller mean error and standard deviation occurs in SA MCC and MCS cases. Greater directional variation in the U.S. LLJ could explain the greater average absolute error in NA. Although the CFM96 average absolute error is small, a further reduced error in SA justifies use of the CFM96 technique to forecast SA MCC and MCS movement.

Table 2. Comparison of observed and forecasted MCC and MCS speeds and directions for both the Cordifi et al. (1996) method for North America (NA) and the author's method developed for South America (SA). Comparison includes standard deviations (Std. Dev.) and average absolute errors. Average absolute errors is the sum of the absolute errors for all cases divided by the total number of events).

	Method for NA (Cordifi et al. method) (based on 103 cases)		Method for SA (author's method) based on 22 cases)	
	MCC or MCS Speed (m s^{-1})			
	Mean	Std. Dev.	Mean	Std. Dev.
Observed	13.6	4.7	13.3	2.9
Forecasted	13.0	3.5	11.9	3.3
Avg. absolute error	2.0	1.8	2.1	1.8
MCC or MCS Direction (degrees)				
	Mean	Std. Dev.	Mean	Std. Dev.
Observed	295.3	32.8	258.7	34.6
Forecasted	294.8	30.7	257.0	29.4
Avg. absolute error	17.2	12.3	16.4	11.8

Average absolute errors in both speed and direction are acceptably small to use in forecasting MCCs and MCSs. The directional average absolute error would, however, yield the greater potential for incorrectly forecasted MCC and MCS placement. An average absolute directional error for SA of 16.4° translates into an average absolute horizontal distance error of 134 km [Avg. observed mean speed x sin (16.4) x 11.5 hrs]. The average lifespan of SA MCCs is 11.5 hours (Velasco and Fritsch 1987). This error indicates the MCC or MCS will be, on average, 134 km from the MCC or MCS forecasted position at 11.5 hours. Of course, re-application of the method throughout the MCC or MCS lifespan will significantly decrease the absolute horizontal error. This error compares very well to the absolute horizontal distance error of roughly 138 km for NA. In spite of the seemingly large distance error, this still places the MCC within its 300 km diameter heavy rain band (CFM96; Maddox et al. 1986).

4. Summary and Concluding Remarks

The CFM96 empirical method for predicting MCC and MCS movement in NA also applies to forecasting MCC and MCS movement in CSA. MCC and MCS movement methods are based on the fact that both advective and propagation components sum to equal the movement of backward or quasi-stationary MCSs, such as MCCs (CFM96; Corfidi 1998). The advective component, defined by the mean motion of individual convective cells, strongly correlates to the mean 850-300 mb cloud layer wind flow. The propagation component, defined by the rate and location of new cell formation relative to existing cells, is related to the LLJ direction.

Application of the procedure to 22 cases (20 of which were MCCs) revealed a correlation coefficient of 0.72 for the observed vs. forecasted MCC and MCS speeds, and a correlation coefficient of 0.81 for the observed vs. forecasted MCC and MCS directions. Mean absolute errors were small enough for the forecasted MCC or MCS centroid location to lie well within the convective system's heavy rain swath. All correlation coefficients, means, variances, and absolute errors for the SA method were comparable to those found in the CFM96 NA method.

This procedure provides a tool to aid in predicting the often elusive propagation component associated with MCSs and MCCs. As in the CFM96 method for NA MCC movement, forecasters can apply this technique only knowing the speed and direction of the mean layer wind and the LLJ. Finally, this technique greatly aids forecasters in predicting the location of heavy rain potential that exists with MCCs and large MCSs.

Although this research provides useful results and an invaluable forecasting technique, there are some shortcomings. The CFM96 method and the SA method presented in this study are both based only on quasi-stationary or backward propagating MCSs such as MCCs. These methods do not apply to forward propagating MCSs such as bow echoes or squall lines (Corfidi 1998). Moreover, this procedure might require further knowledge of the system relative convergence that may not necessarily correspond to the LLJ direction (Corfidi 1998). In addition, this research utilized a subjective determination of the cold shield centroid from GOES IR imagery at three-hour intervals. Exploiting shorter intervals or satellite imagery with higher resolution may yield more precise MCC or storm cell locations. Finally, the lack of spatial resolution of the upper air observing network over SA may contribute to slightly less accurate upper air analyses and cloud layer component calculations. Incorporating satellite derived observations into the upper air network, and eventually into computer forecasting models, should improve the accuracy of both empirical and model forecasts of MCC movements.

Acknowledgments

The author sincerely thanks Michel Davison of the International Desks section of NCEP for providing necessary background information and satellite imagery of MCCs in SA. Special thanks are extended to Lt. Col. Michael Walters and Major Robin N. Benton of the Air Force Institute of Technology (AFIT) for providing meteorological and statistical expertise. A very special thanks is extended to Ms. Kathleen Collins, a summer intern from Ball State University at the Air Force Institute of Technology, for her editing and formatting assistance with the manuscript. This research represents a portion of the author's Master's thesis completed at AFIT.

Authors

Marc Gasbarro is a Captain for the U.S. Air Force, where he currently serves as Staff Weather Officer for the Electronics System Center at Hanscom AFB MA. His previous military assignments include Flight Commander, Base Weather Station, 355th Wing and Southwest Regional Flight Commander, 25th Operational Weather Squadron both at Davis-Monthan AFB AZ, and Wing Weather Officer, 75th Air Base Wing at Hill AFB UT. He also deployed to Combat Weather Teams at Prince Sultan Air Base, Kingdom of Saudi Arabia, and Al Udeid Air Base, Qatar. He received his B.S. in Meteorology (1995) from Lyndon State College, VT and M.S. in Meteorology (2003) from Air Force Institute of Technology at Wright-Patterson AFB, OH. Email: Marc.Gasbarro @hanscom.af.mil

Stephen Corfidi has been a lead forecaster with the NOAA-NWS Storm Prediction Center (SPC) since 1994. Steve's prior associations include NOAA-NWS's Hydrometeorological Prediction Center, National Severe Storms Forecast Center, Baltimore-Washington National Weather Service Forecast Office and Meteorological Development Laboratory (formerly Techniques Development Laboratory). He received his B.S. in Meteorology (1981) and M.S. in Meteorology (1994) from Pennsylvania State University.

Ronald Lowther is a Colonel in the U.S. Air Force where he currently serves as Director of Air and Space Science, Headquarters Air Force Weather Agency, Offutt AFB NE. His previous military assignments include Deputy Head and Assistant Professor of Atmospheric Physics, Department of Engineering Physics, Air Force Institute of Technology, Wright-Patterson AFB OH; Assistant Director of Operations, Air Force Combat Climatology Center, Asheville, NC; Department of Defense Climatologist, Headquarters U.S. Air Force, Washington, DC; Special Project Analyst and Manager of Special Access Programs, Air Force Environmental Technical Applications Center, Scott AFB IL; Wing Weather Officer, 487th Cruise Missile Wing, Comiso Air Base, Italy, and Weather Officer, 15th Air Force Operations Center, March AFB CA. He received his B.S. in Computer Science (1983) from Chapman University, CA and M.S. in Meteorology (1989) and Ph. D. in Meteorology (1998) from Texas A&M University.

References

Bonner, W. L., 1968: Climatology of the Low-Level Jet. *Mon. Wea. Rev.,* 96, 833-850.

CIRA, cited 2002: GOES-8, 3-hourly, Channel 4 IR, 2002 imagery. [Available from Cooperative Institute for Research in the Atmosphere, Colorado State University, Foothills Campus, Fort Collins, CO 80523-1375].

Corfidi, S. F., J. M. Fritsch, and J. H. Merritt, 1996: Predicting the movement of mesoscale convective complexes. *Wea. Forecasting,* 11, 41-46.

_____, 1998: Forecasting MCS mode and motion. Preprints, *19th Conf. on Severe Local Storms,* Minneapolis, MN, *Amer. Meteor. Soc.,* 626-629.

Davison, M., 1999: Mesoscale Systems over South America. [Available from International Desks, NOAA/National Centers for Environmental Prediction, Hydrometeorological Prediction Center/ Development and Training Branch, 5200 Auth Rd., Camp Springs, MD 20746].

_____, 2002: Mesoscale Convective Case Studies. [Available from International Desks, NOAA/National Centers for Environmental Prediction, Hydrometeorological Prediction Center/Development and Training Branch, 5200 Auth Rd., Camp Springs, MD 20746].

Gasbarro, M. R., 2003: Forecasting excessive rainfall and low cloud bases east of the Northern Andes and mesoscale convective complex movement in Central South America. M.S. thesis, Dept. of Engineering Physics, Air Force Institute of Technology, 163 pp. [Available from Air Force Institute of Technology, 2950 Hobson Way, Wright-Patterson AFB OH 45433].

Lenters, J. D., and K. H. Cook, 1999: Summertime precipitation variability over South America: Role of the large-scale circulation. *Mon. Wea. Rev.,* 127, 409-431.

Maddox, R. A., 1980: Mesoscale Convective Complexes. *Bull. Amer. Meteor. Soc.,* 61, 1374-1387.

_____, D. L. Bartels, K. W. Howard, and D. M. Rodgers, 1986: Mesoscale Convective Complexes in the middle latitudes. *Mesoscale Meteorology and Forecasting*, P. S. Ray, Ed., American Meteorological Society, 390-413.

Saulo, A. C., S. C. Chou, and M. Nicolini, 2000: Model characterization of the South American low-level flow during the 1997-1998 spring-summer season. *Climate Dyn.,* 16, 867-881.

Snyder, J. P., 1987: *Map Projections – A Working Manual.* US Geological Survey Professional Paper 1395, 383 pp.

Velasco, I., and J. M. Fritsch, 1987: Mesoscale Convective Complexes in the Americas. *J. Geophys. Res.,* 92, 9591-9613.